## SUPPLEMENTAL FIGURES

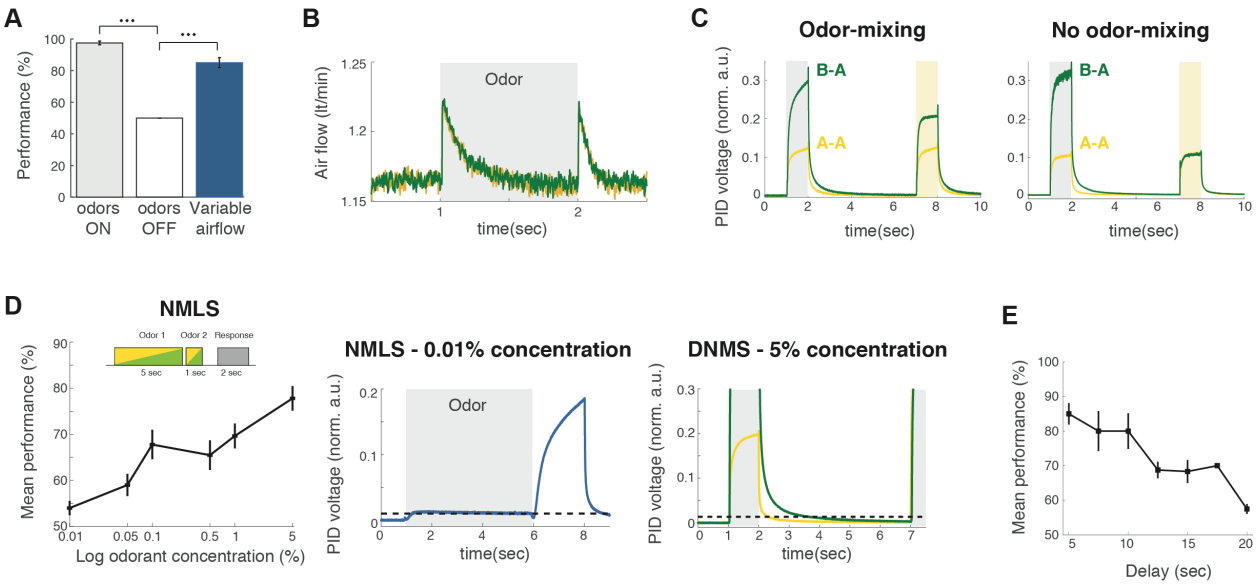


**Figure S1: Controlling odor delivery and mouse performance. A.** Mean ± SE performance of mice (N = 2) during default sessions (grey), sessions with no odors (white) and sessions with variable airflow values (blue). In sessions without odors, mice never licked for reward, performing at chance level (asterisks: $P < 0.001$, WT). **B.** Mean airflow measurements before, during (grey) and after odor delivery. Yellow: odor-A (isoamyl acetate). Green: odor-B (pinene). Odor-delivery exhibits similar airflow profiles for both odors and their baseline is similar to that of clean air before and after delivery. **C.** Left: Example of mean PID measurement of all B-A and A-A trials in a session where the set up allowed odor-mixing to occur in the tubes (long common odor-path between two odorants). PID measurement during the second odor-A delivery (yellow box) is much higher in B-A trials (contaminated with lingering odor-B in the tubes). Left: Similar measurement for our default set up without odor-mixing. Second odor-A measurement is the same irrelevantly of the first odor. **D.** Left. Mean ± SE performance during the NMLS task, as a function of the odorant concentration used for the long stimulus (N = 3 mice). Schematic indicates the task structure. Mice reached near-chance levels at 0.01% odorant concentration. Middle: Mean PID measurement in 0.01%-concentration trials. Dashed line: PID-baseline during the long-odor delivery (grey). Right: Mean PID measurement during all trials starting with odor-A (yellow) or odor-B (green) in default 5%-concentration DNMS trials. Dashed line: 0.01%-baseline. PID measurement during odor-B is truncated for plotting clarity. **E.** Mean ± SE performance during sessions of increasing delay durations (N = 4 mice). Performance decline is indicative of working-memory tasks, and excludes performance confounds by odorized air lingering within air-valves.

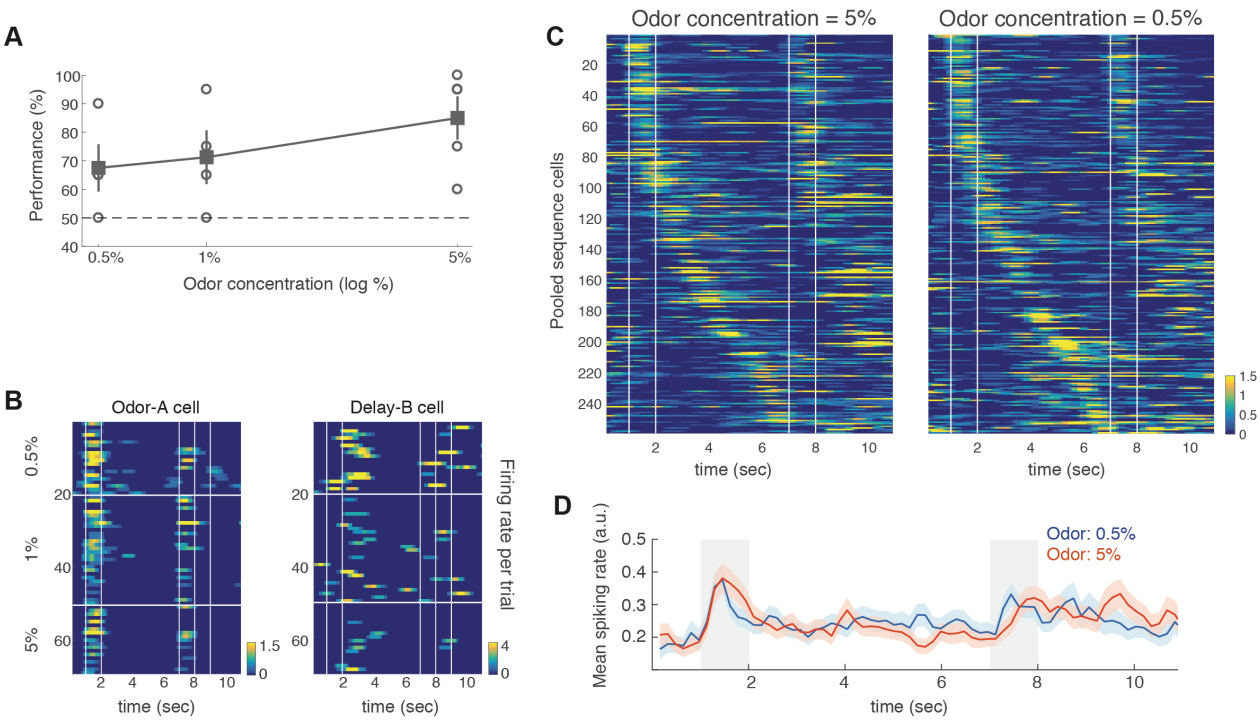


**Figure S2: Spike sequences do not encode odor-concentration. A.** Individual performances (dots) and mean ± SE over sessions with 3 different odorant concentrations (N = 3 mice). **B.** Example odor-A and odor-B cell firing rates during their respective preferred-trials for the three concentrations. **C.** Pooled sequence-cell firing rates over 5% and 0.5% odor concentration trials. Sequential spiking remains intact indicating that cells do not encode odorant concentration. **D.** Mean ± SE firing rate of sequence-cells for 5% and 0.5% concentrations. No significant differences were found at any time point ($P > 0.05$, WT) Grey bars: Odor delivery.

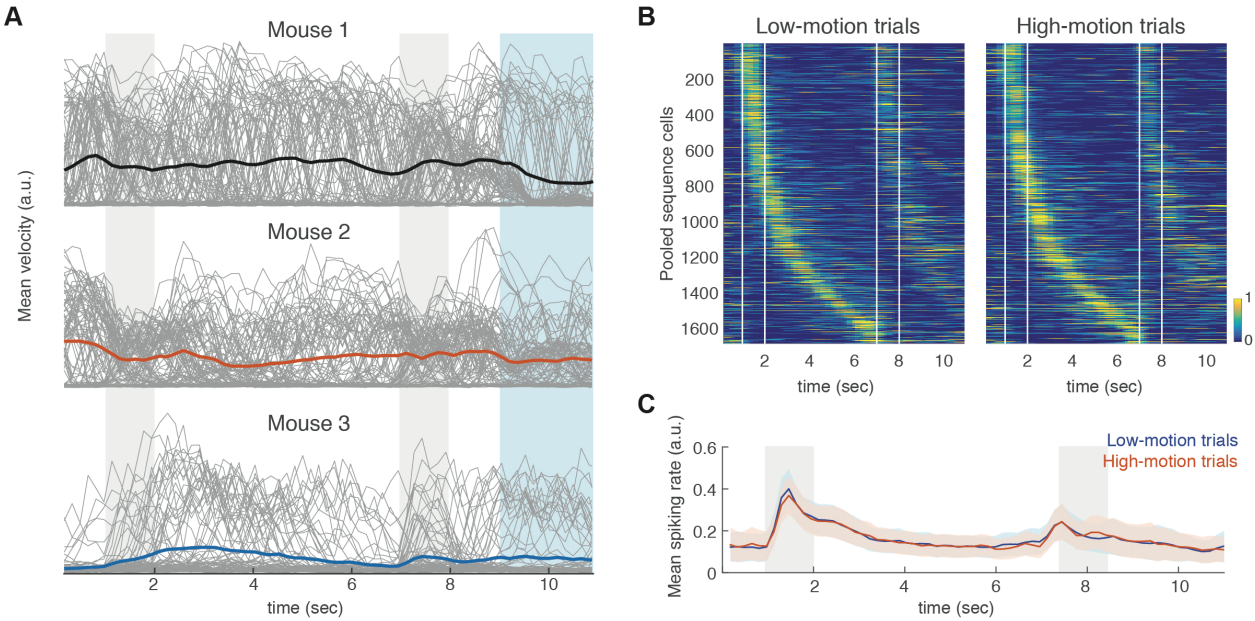


**Figure S3: Spike sequences do not encode motion on the treadmill. A.** Example mean velocity profiles from three mice averaged over all trials in a recording day. Some animals exhibited non-specific motion during the trial (black), whereas others tended to halt during odor presentation (orange) or accelerate during and after odor presentation (blue). Gray traces indicate individual trials. Grey bars: Odor delivery. Blue bars: Response window. **B.** Pooled sequence firing rates from all well-trained sessions, during 30% trials with the lowest average motion (left) versus 30% trials with the highest motion (right). Both groups display similar sequence activity. **C.** Mean±SE spiking rates of sequence-cells, averaged over low- and high-motion trials in all well-trained sessions. Line indicates average over all sessions. No significant differences exist at any time point ($P > 0.05$; WT). Grey bars: Odor delivery.

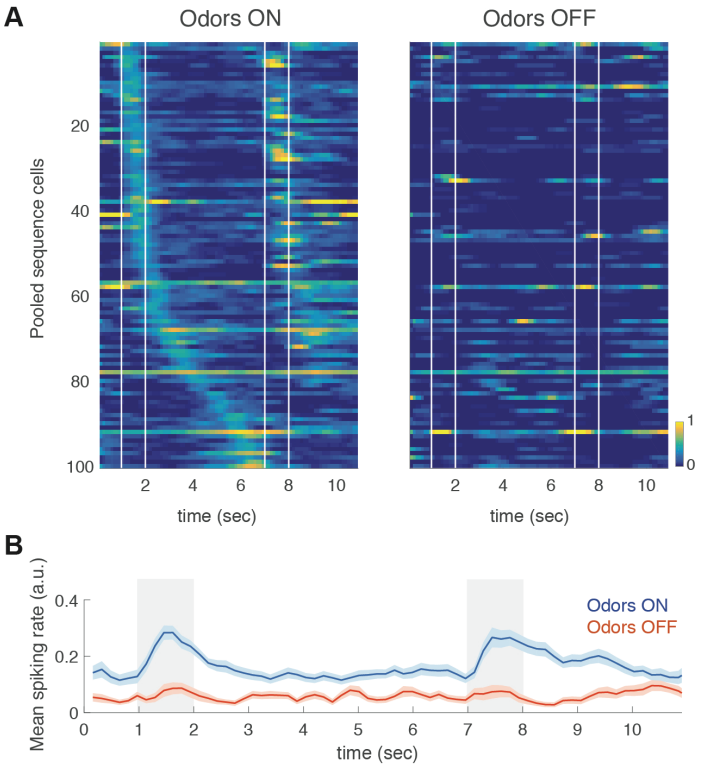


**Figure S4: Spike sequences do not encode auditory cues. A.** Pooled sequence-cell firing rates over default preferred-trials followed by trials with the odors turned off (N = 3 mice) but all valve auditory cues present. **B.** Mean $\pm$ SE firing rates of sequence-cells for the two cases are significantly different at all time points ($P < 0.05$; WT, FDR). Grey bars: Odor delivery.

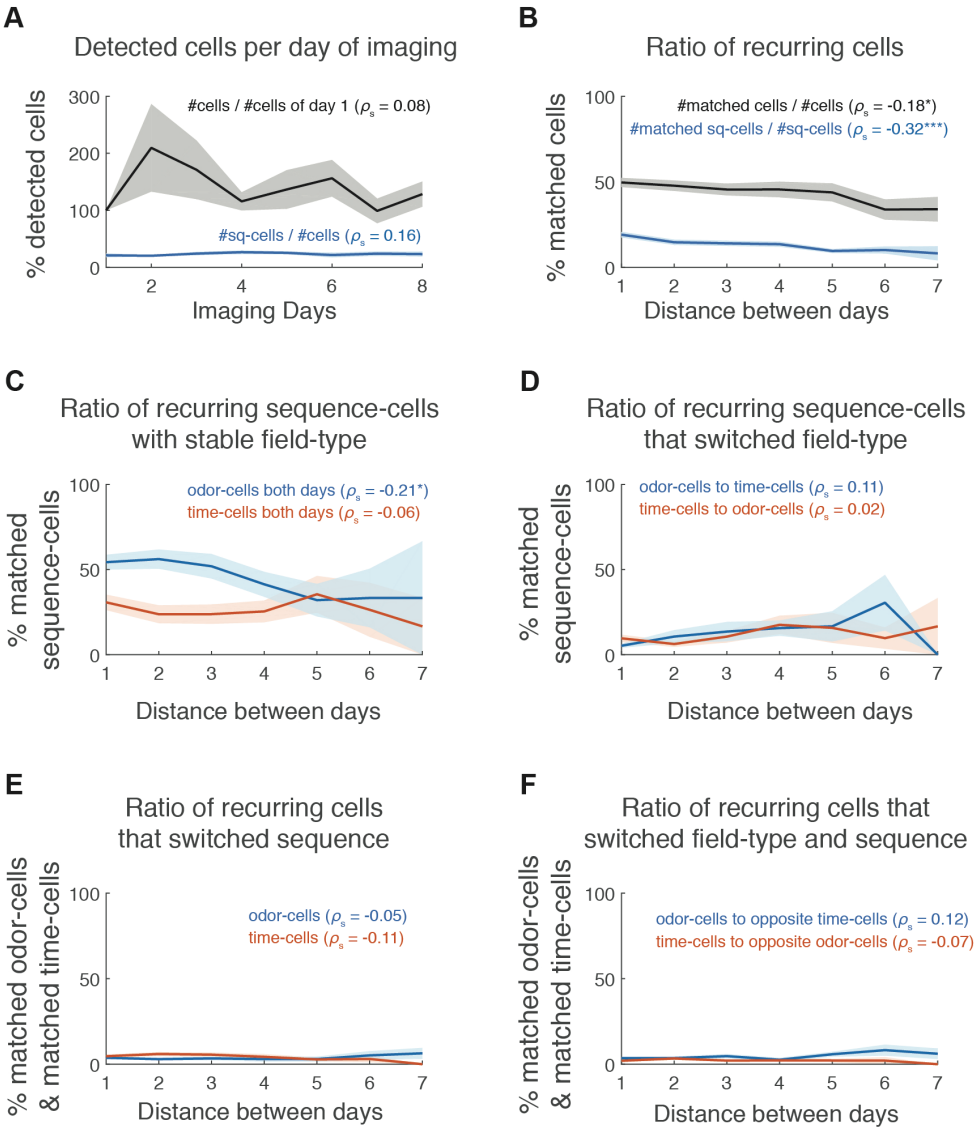


**Figure S5: Registered cells and sequence-cell shifts across days.** **A.** Ratio of detected ROI in each animal over ROI detected on its first day of imaging (grey) and ratio of sequence-cells over all ROI per day (blue). Both numbers remain stable throughout imaging for up to a week. **B.** Ratio of each day's ROI that were matched with ROI from another imaging day, as a function of distance between days (grey). Same for ratio of sequence-cells (of the same sequence) that were matched between the two days (blue). **C.** Ratio of matched sequence-cells between two days that were odor-cells or time-cells in both days, as a function of distance between days. **D.** Same as **C** for ratio of matched sequence-cells that switched their field-type from odor to time or vice versa. **E.** Ratio of matched odor-cells and time-cells between two days that remained odor- or time-cells respectively, but switched their sequence, as a function of distance between days. **F.** Same as **E**, for those that switched both their field-type and sequence. $\rho_S$ : Spearman correlation. Asterisks: * P < 005; *** P < 0.001, permutation distribution test.

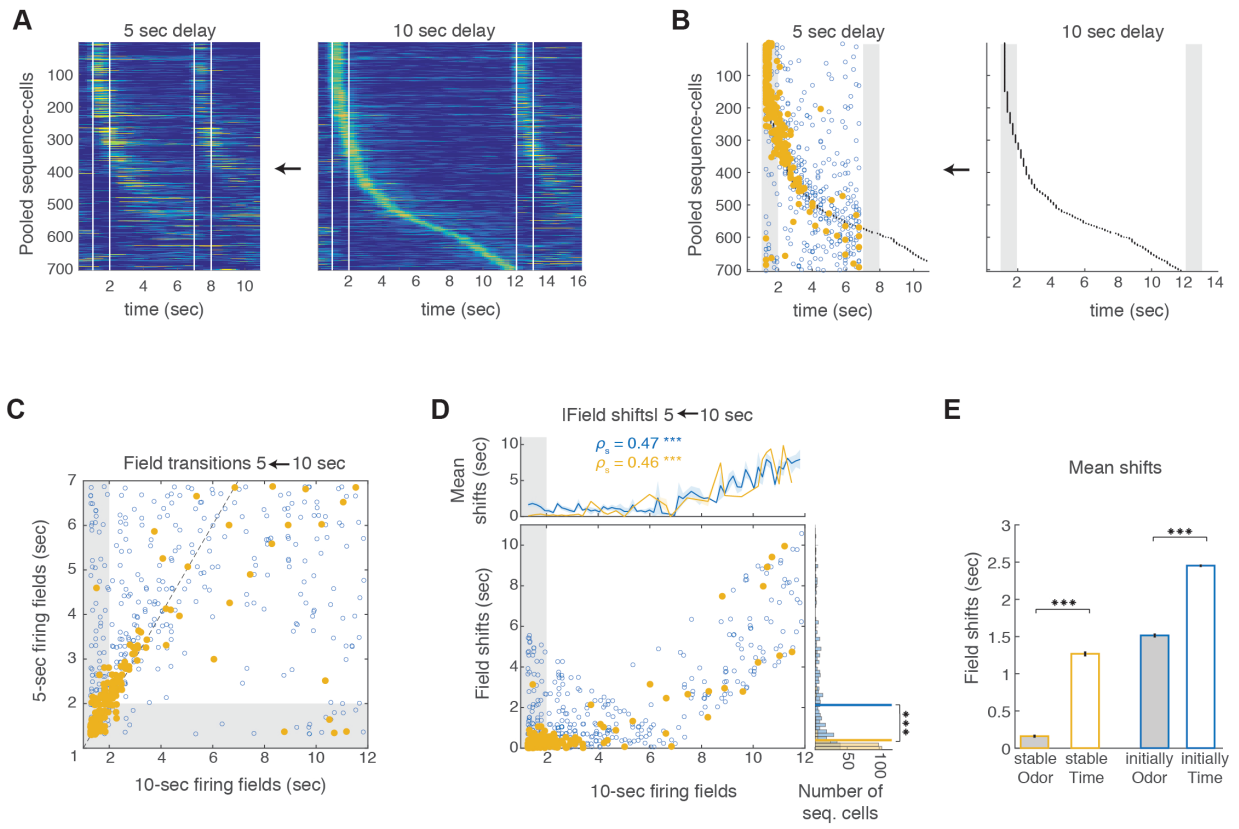


**Figure S6: Odor-cells retain their field whereas time-cells shift their fields when extending the delay period. A-B.** Pooled sequence-cells from all recording days that included 5 sec and 10 sec delay sessions on the same day (N = 10 days). The 10 sec delay sessions were used to detect sequence-cells (right). Their rate (**A**) and field locations (**B**) over both 5 sec (left) and 10 sec delay sessions (right) are shown as in Figure 5. **C**. Time bin of each cell's mean firing rate peak over 5 sec delay sessions as a function of their 10 sec delay field (blue circles). Yellow dots: Cells with significant fields at those bins in 5 sec delay. Dashed line indicates no change in firing field. **D.** Absolute time shifts of sequence-cells between 5 and 10 sec delay sessions as a function of their 10 sec delay field. Top: Mean $\pm$ SE shifts as a function of a cell's 10 sec field. Colors as before. $\rho_s$: Spearman correlation; asterisks: $P < 0.001$, permutation distribution. Right: Histogram of sequence-cells' field shifts. Lines indicate distribution means. Asterisks: $P < 0.001$, two-sample Kolmogorov-Smirnov test. **E.** Mean $\pm$ SE shifts of odor-cells (grey bars) versus time-cells (white bars) for all common sequence-cells between 5 sec and 10 sec delay sessions (yellow; $P < 0.001$, WT) and 10 sec-only sequence-cells (blue outline; $P < 0.001$, two-sample t-test, Bonferroni over the two tests).

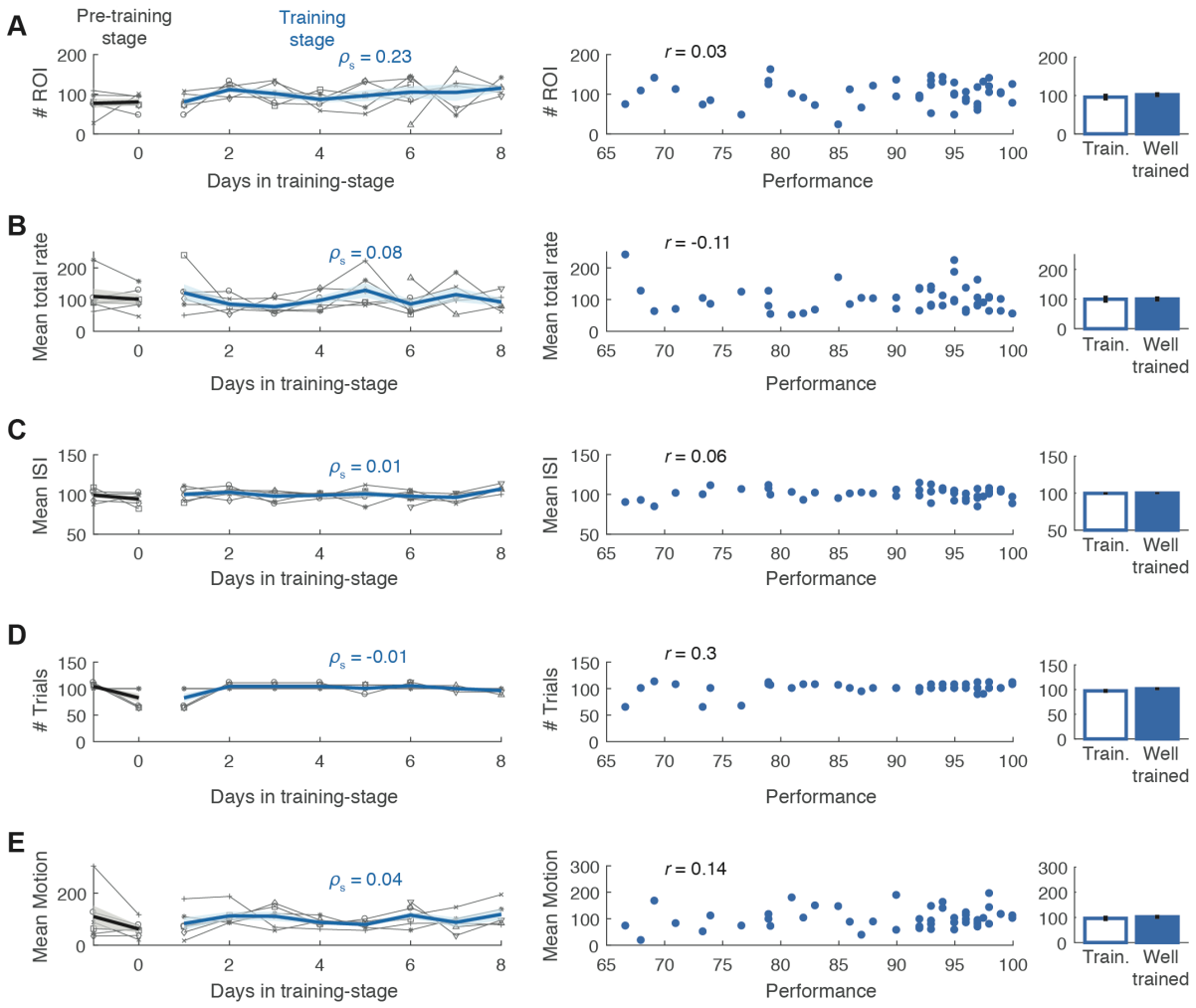


**Figure S7: Correlations between time cells and performance are not affected by imaging, spiking or motion confounds. A.** Left: Total number of active ROI as a function of consecutive days in the final training-stage, plotted as in Figure 6 (N = 8 mice). Two imaging days in the pre-training stage are also shown (N = 6 mice; black). ROI are normalized over their mean number across all training-stage days, separately in each mouse (shown in percentage). $\rho_S$: Spearman correlation. Middle: Normalized number of ROI versus mouse's daily mean performance. *r*: Pearson correlation. Right: Mean normalized number of ROI during all days at 'training level' (<90% mean performance) versus 'well-trained' level (≥90%). **B-E**. Same as in **A** for mean summed firing rate of all ROI per day (**B**), mean interspike interval (**C**), number or trials per imaging day (**D**), and mean summed motion over trials (**E**). All measures are normalized as in **A**. No significant Spearman correlations over imaging days, Pearson correlations with performance or differences between trainining – well trained levels were observed (P > 0.05; permutation distribution and WT respectively; FDR over all corresponding comparisons).

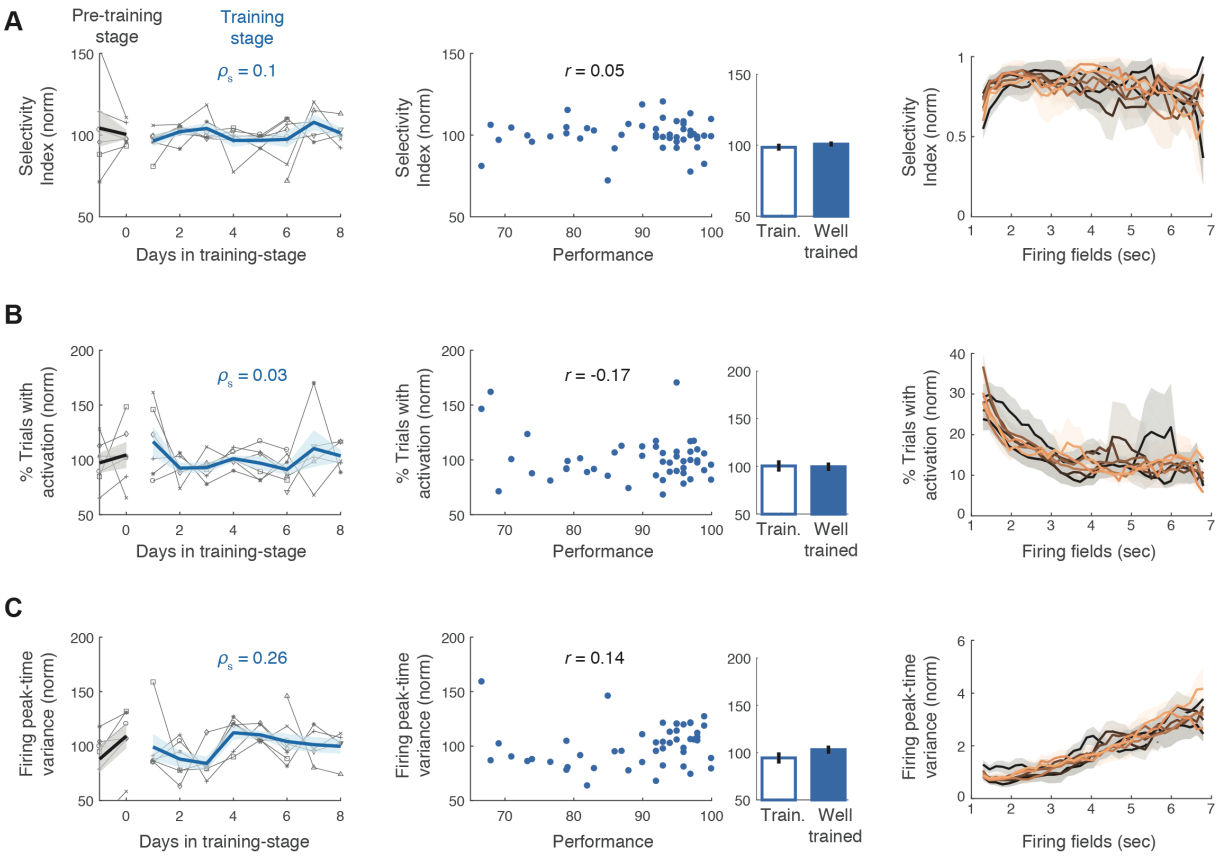


**Figure S8: Spiking properties of sequence-cells do not change over days or with performance improvement. A.** Same plotting scheme as in Figure S7 for mean selectivity index of sequence-cells each day. Rightmost panel: Distribution of mean ± SE selectivity index as a function of firing fields for each day (color coded as in Figure 7D). **B-C**. Same as in **A** for activation (% of preferred trials where a cell spiked; **B**) and variance of maximal spiking time-bin (**C**) of all sequence-cells. No significant correlations or differences were observed (P > 0.05; permutation distribution and WT respectively; FDR over all corresponding comparisons).

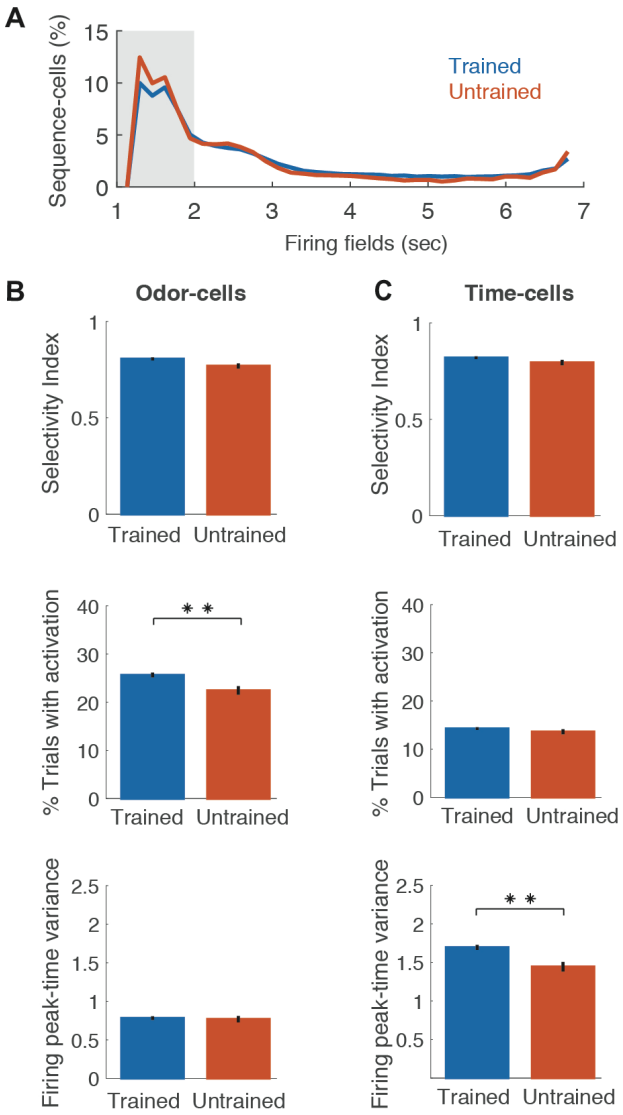


**Figure S9: Field distribution and spiking properties of sequence-cells in trained and untrained animals. A.** Normalized distribution of firing fields (% over all sequence-cells) in trained and untrained animals. Both groups exhibited similar distributions of time-fields. **B**. Mean ± SE selectivity index (top), activation (middle) and variance of maximal spiking time-bin (bottom) of odor-cells in trained versus untrained animals. Only the participation exhibited a small but significance decrease in untrained animals ($P < 0.01$; WT; FDR). **C.** Same as **B** for time-cells. Both groups exhibited similar properties with the exception of a small but significant decrease in spiking variance in untrained animals ($P < 0.01$; WT; FDR).